Paired helix scanning distinguishes structural requirements for amphipathic peptide scaffold functions

John S. Albin[1,2,3] and Bradley L. Pentelute[1,4-6*]

[1]Department of Chemistry, Massachusetts Institute of Technology, Cambridge, MA, 02139, USA

[2]Division of Infectious Diseases, Massachusetts General Hospital, Boston, MA, 02114, USA

[3]Harvard Medical School, Boston, MA, 02115, USA

[4]The Koch Institute for Integrative Cancer Research, Massachusetts Institute of Technology, Cambridge, MA 02142, USA

[5]Center for Environmental Health Sciences, Massachusetts Institute of Technology, Cambridge, MA 02139, USA

[6]Broad Institute of MIT and Harvard, Cambridge, MA 02142, USA

*Correspondence, Lead Contact: jalbin@mgh.harvard.edu

Summary: Mammalian cell toxicity is a major barrier to the development amphipathic helical peptides for antibiotic applications. Toward addressing this limitation, we report here the development of a paired Ala-Aib helix scanning approach to isolate the sidechain-independent effects of helical content on the underlying antimicrobial and hemolytic activities of a model cathelicidin-derived scaffold. Despite the generally accepted premise that cathelicidin helical content correlates with antimicrobial activity, we find that this relationship is species-dependent. Moreover, gains in antimicrobial activity associated with greater helical content generally outpace losses associated with increasing hemolytic activity. Combining these insights with our prior work on the development of oligomerization-deficient cathelicidins, we develop a short Aib-rich cathelicidin derivative with a 32-fold improvement in *in vitro* therapeutic index over the naturally occurring parent helix. Our results thus introduce principles for the rational design of cathelicidin-derived scaffolds based on differential structural requirements for distinct functions.

Keywords: amphipathic peptide, amphipathic helix, antimicrobial peptide, host defense peptide, cathelicidin, Aib, aminoisobutyric acid

Introduction

Antimicrobial resistance is a growing source of global morbidity and mortality, accounting for more than 1 million deaths per year in recent years with the potential to become the single largest cause of death worldwide in the coming decades[1–3]. One strategy to counteract the growing threat posed by antimicrobial resistance is to derive new chemical entities by mining and developing natural product host defense peptides (HDPs), which despite their potential have yet to reach clinical use[4–11].

Humans express a variety of structurally diverse HDPs, including α defensins, β defensins, histatins, neuropeptides, and a number of miscellaneous protein cleavage products that have varying degrees of reported antimicrobial activity against different microbes[12–14]. Humans also express a single cathelicidin, initially as a pro-peptide packaged within neutrophil granules, which undergoes cleavage to form the active peptide LL-37[15–17]. In its active form, LL-37 is a prototypical amphipathic helix that is thought to act through membrane disruption, though we have recently reported results to suggest that other mechanisms may contribute to its antimicrobial activity[18,19]. Regardless, the antimicrobial activity of LL-37 is thought to be dependent upon its helical structure, rendering this a valuable model in which to study associations between helical structure and functional phenotypes[20–23].

Many prior reports have described the activities of diverse fragments of LL-37. Among these fragments, KR-12 spanning residues 18-29 of full-length LL-37 is generally regarded as the minimal unit of LL-37 activity[21,22,24–31]. Building on this work, we have recently used rational design principles involving the transposition of an LL-37 N-terminal biphenyl motif onto the KR-12 core to yield a short cathelicidin called FF-14 with >16-fold greater activity against gram-negative bacteria[32]. In related work, we have also identified mutations in the LL-37 oligomerization interface, I24 and L28, that drive LL-37 hemolytic activity[33]. Each of these oligomerization drivers is also found in FF-14 at positions I9 and L13, and thus may also contribute to the hemolytic activity of this short cathelicidin derivative.

Toward better understanding and harnessing the structural principles underlying cathelicidin phenotypes, we describe here a systematic structural scan of the FF-14 helix using paired mutagenesis with Ala or the sidechain-equivalent helix-promoting α,α-disubstituted noncanonical amino acid aminoisobutyric acid (Aib)[34–37]. Our results show that, although Aib can promote helical structure, this size of this effect is context-dependent and thus vulnerable to emergent interactions within a short primary sequence. We further demonstrate that the expected correlation between helical content and activity against *Escherichia coli* does not hold in the instance of a distinct gram-negative species, *Pseudomonas aeruginosa*, with intermediate effects on hemolytic activity between these extremes. Thus, the impact of helical content on cathelicidin functions depends both on sequence context and on the function being assayed, implying distinct contributions of helical structure to each phenotype. Finally, we build on these findings to make an Aib-rich derivative of FF-14 that retains helical structure and activity against *E. coli* while blunting hemolytic activity, resulting in a derivative with a 32-fold increase in *in vitro* therapeutic index compared with the naturally occurring parent peptide. Our work thus establishes principles for the rational development of short cathelicidin derivatives that leverage the distinct structural drivers of antimicrobial and hemolytic activity.

Results

Antimicrobial and hemolytic activity correlate in grouped Ala mutants of FF-14

Our prior structure-activity studies of full-length LL-37 rest on the hypothesis that distinct surfaces of LL-37 contribute to distinct functions. To test this, we carried out grouped Ala mutagenesis in which multiple structurally contiguous residues were changed to Ala simultaneously and then assessed for changes in phenotype. This approach works in LL-37 because this template retains strong helical content despite extensive Ala substitutions. An important finding of this work is that derivatives with substitutions at key residues in a previously-described oligomerization interface in LL-37[38,39], particularly I24 and L28, have diminished hemolytic activity, thus effectively detoxifying this as a lead antimicrobial[33].

To determine whether it would be possible to achieve this same separation of function in the FF-14 template, we first made a series of grouped Ala mutants corresponding to those initially described in full-length LL-37. That is, any position that occurs both in LL-37 and in FF-14 is substituted in a pattern identical to that used previously in LL-37[33]. We further made paired versions of these mutants in which the first two amino acids of the 14-mer with a given substitution pattern were either the wild-type LL-37 residues [EF] or the biphenyl motif residues [FF] that confer increased activity on FF-14[32]. As shown in **Figure 1A-B**, activity of these grouped Ala mutants against *E. coli* and *Pseudomonas* was universally attenuated in mutants starting with [EF]. Although substitution with the biphenyl motif [FF] rescued antimicrobial activity in m6 and, to a lesser extent, m5, this also resulted in increased hemolytic activity as shown in **Figure 1C**. Importantly, however, mutants corresponding to m4 substitutions, which include the oligomerization-associated residues I9 and L13, lacked both antimicrobial and hemolytic activity. Thus, antimicrobial and hemolytic activity profiles in FF-14 derivatives remain coupled. This stands in contrast with the ability of LL-37 m4 and of the control antibiotic colistin to separate antibacterial and hemolytic functions. Mutants used in these studies are shown in **Figure 1D**.

Both helical content and sidechain identity contribute to function

Based on the results of **Figure 1**, we hypothesized that loss of function in FF-14 derivatives might be due to an associated loss of helical content in the context of multiple amino acid substitutions. To test this, we analyzed these mutants by circular dichroism (CD) spectroscopy. Spectra for each mutant are shown in **Supplementary Figure 1A-G**. Helical content as calculated using BeStSel[40] is summarized in **Supplementary Figure 1H**. Although some mutants such as FF-14 m4 and FF-14 m4-FF appear to lose structure, the remaining grouped mutants retain at least intermediate helical character, where activity profiles appear driven more by the biphenyl motif at the first two positions than by helical content itself, consistent with our initial description of this scaffold[32]. Thus, although helical content can contribute to activity profiles in these mutants, sidechain identities can also drive function, which poses intrinsic challenges to our ability to distinguish the contributions of helical content and sidechain identity to a given function. We therefore proceeded to a more systematic evaluation of individual positions in the FF-14 scaffold.

Supplementary Figure 2 shows the data from **Figure 1** in histogram format including error bars. The kinetic curves associated with the endpoint data provided in **Figure 1** are shown in **Supplementary Figures 3-14** (antimicrobial susceptibility testing) and **Supplementary Figures 15-26** (hemolysis assays). A standardized, quantitative presentation of **Figure 1** data is provided in **Supplementary Table 1**.

Antimicrobial and hemolytic activity correlate in single Ala mutants of FF-14

In our prior work on LL-37, we have found that full-length LL-37 tolerates up to at least eight simultaneous Ala mutants out of the 37-mer sequence without substantial loss of helical structure[33]. Based on the results of **Figure 1**, however, FF-14 appeared less tolerant of such alterations. We therefore hypothesized that FF-14 scaffold might better tolerate single Ala

mutations to separate antimicrobial and hemolytic activities, particularly within the detoxifying m4 oligomerization interface, and proceeded to make a series of single Ala mutants covering the FF-14 sequence.

Antimicrobial susceptibility testing with these mutants against *E. coli* as shown in **Figure 2A** demonstrated modest improvement in activity with mutants R8A and D11A, the latter in particular echoing prior similar evaluations in the context of KR-12[29]. While mutant D11A also showed improved activity against *Pseudomonas* in **Figure 2B**, R8A demonstrated an increased MIC against this distinct gram-negative species. As shown in **Figure 2C**, hemolytic activity generally tracked with activity against *E. coli*. For example, the greatest losses in antimicrobial activity against *E. coli* in **Figure 1A** localized to I9A and L13A, corresponding to the oligomerization interface residues primarily responsible for separation of antibacterial and hemolytic activity in full-length LL-37, I24 and L28[33]. Thus, individual Ala mutations did not reveal a means by which to separate antimicrobial and hemolytic functions in FF-14.

Supplementary Figure 27 shows the data from **Figure 2** in histogram format including error bars. The kinetic curves associated with the endpoint data provided in **Figure 2** are shown in **Supplementary Figures 28-42** (antimicrobial susceptibility testing) and **Supplementary Figures 43-57** (hemolysis assays). A standardized, quantitative presentation of **Figure 2** data is provided in **Supplementary Table 2**.

Modest correlation between antimicrobial activity and FF-14 Ala mutant helical content

Based on the loss of helical content associated with FF-14 m4 grouped mutants in **Figure 1** and **Supplementary Figure 1**, we hypothesized that helical content might correlate with antimicrobial activity among single Ala mutants. To directly assess this, we again collected CD spectra from each of the single Ala mutants used in **Figure 2**. As shown in **Supplementary Figure 58**, strong or absent helical content was generally associated with strong or weak antimicrobial activity, respectively. For example, the R8A and D11A mutants are strongly helical

and more active than wild-type FF-14 against *E. coli*, while the I9A and L13A mutants are disordered and largely inactive. Incorporating the middle of this range, however, shows only a modest correlation among the calculated percent helical content in these mutants in comparison with the log2 of their MIC against *E. coli*. Thus, helical content appears predictive of activity at the extremes, but less so for intermediate values. It is unclear whether distinctions in this middle range reflect quantitative limitations of the assays used or true biology. Overall, however, these results are generally consistent with prior studies demonstrating the importance of helical structure for LL-37 activity[17,20]. Individual spectra are provided in **Supplementary Figure 59**.

Aminoisobutyric acid (Aib) incorporation improves cathelicidin activity against *E. coli* but not *Pseudomonas*

In the context of full-length LL-37, the combination of I24A and L28A largely recapitulates the separation of function phenotype of the LL-37 m4 mutant. The equivalent positions in FF-14 are I9 and L13, both of which lose both structure and activity when changed to Ala in **Figure 2**. One method of better supporting structure in helical peptides is to incorporate α,α-disubstituted amino acids such as Aib (*e.g.*, [41,42]), which is also a prominent feature in helical fungal natural product peptaibols[43–46]. We therefore reasoned that generating a single mutant Aib dataset corresponding to the Ala mutants in **Figure 2** would allow us to isolate the structure-specific requirements underlying FF-14 functions independent of sidechain identity, which may in turn highlight a pathway to rationally incorporating modifications at residues I9 and L13 to separate antimicrobial and hemolytic activity.

To test this hypothesis, we completed a structural scan of FF-14 in which we used Aib to replace each residue in FF-14 rather than Ala, thus maintaining sidechain equivalence while introducing conformational restriction. As shown in **Figures 3A-B** and **Supplementary Table 3**, antimicrobial activity with Aib substitution was neutral-to-improved against *E. coli* at all residues relative to Ala. This was particularly true of F2, I5, and I9, where substitution of Aib in place of

Ala results in 8-fold improvements in MIC against *E. coli*. Despite these improvements against *E. coli*, the effect of Aib substitution on MICs against *Pseudomonas* was generally neutral, while hemolytic activity was typically neutral-to-increased among Aib mutants (**Figure 3C**). A summary of the mutants used in these studies is shown in **Figure 3D**. Thus, the sidechain-neutral conformational constraints introduced by Aib exert their primary effects at the level of FF-14 activity against *E. coli*, with lesser effects on hemolytic activity and no substantial effect on antimicrobial activity against *Pseudomonas*.

Supplementary Figure 60 shows the data from **Figure 3** in histogram format including error bars. The kinetic curves associated with the endpoint data provided in **Figure 3** are shown in **Supplementary Figures 61-76** (antimicrobial susceptibility testing) and **Supplementary Figures 77-92** (hemolysis assays). A standardized, quantitative presentation of **Figure 3** data is provided in **Supplementary Table 3**.

Paired Ala-Aib scanning distinguishes the effects of helical content on FF-14 functions

Building on the comprehensive dataset generated in the course of **Figures 2-3**, we next asked whether it might be possible to derive general principles about the relationships between FF-14 structure and associated functions through a more explicit comparison of the effects of introducing conformational restriction at each residue. **Table 1** summarizes quantitative changes in helical content, antimicrobial activity, hemolytic activity, and the ratio of hemolytic to antimicrobial activity for a matched set of Ala versus Aib substitutions along the length of the FF-14 scaffold.

Overall helical content increased an average of 3.2-fold with Aib substitution, which was mirrored by an average 3.3-fold improvement in antimicrobial activity against *E. coli* among Aib mutants. This effect on helical content was not evenly distributed throughout the scaffold, however, but rather appeared partially dependent on local sequence context, with a range of fold-changes from 0.7-6.7. Moreover, the strongest effects on helical content were seen both on

the hydrophobic (*e.g.*, I9 6.7-fold and V6 5.3-fold) and hydrophilic (*e.g.*, K10 5.6-fold and R14 4.6-fold) surfaces. Within the FF-14 scaffold, then, Aib incorporation universally resulted in increased observed helical content. The size of this effect, however, appeared strongly influenced by local sequence context. Consistent with prior literature, activity against *E. coli* tracked closely with helical content.

Despite the three-fold changes in helical content and antimicrobial activity against *E. coli* effected by substitution with Aib over Ala, the average effect of Aib substitution on antimicrobial activity against *Pseudomonas* was neutral. Thus, despite clear precedent in the literature for a correlation between helical structure and antimicrobial activity, this effect may differ by species. This may suggest a pathway by which to pursue the rational design of cathelicidin derivatives leveraging structurally distinct activity determinants. Consistent with differential effects of helical content on different target cell types, hemolytic activity among Aib substituted mutants increased 2-fold compared with Ala, staking out an intermediate position between effects on *E. coli* and effects on *Pseudomonas*. The net effect of Aib substitution on *in vitro* therapeutic index is thus a modest 1.6-fold average improvement, following the standardized convention in **Supplementary Tables 1-5** for calculating this value as hemolytic activity divided by the MIC against *E. coli*. CD spectra for Aib-substituted mutants are shown in **Supplementary Figure 93**.

Improved therapeutic index of selected combinatorial Aib substitutions

Given the ability of single Aib mutants to promote helical structure, we reasoned that double mutants might yield further improvements, particularly where each individual residue was found in **Table 1** to promote helical content. To test this hypothesis, we made a series of four dual Aib substitutions at *i,i+4* positions covering all possible combinations with this spacing along the helical hydrophobic surface (1+5, 2+6, 5+9, and 9+13). Among these, all except for I9B+L13B retained appreciable activity against *E. coli* (**Figure 4A**), with F2B+V6B being the most active. These also generally retained strong helical character, again with the exception of

I9B+L13B (**Supplementary Figure 94**). Reinforcing the context dependence of these substitutions, however, we noted that the effects of multiple Aib substitutions on helical content were not additive. That is, the helical content of some double mutants was diminished relative to the best of their individual substitutions – *e.g.*, I5B is 91.6% helical, but I5B+I9B is 72.3% helical; I9B is 54% helical while I9B+L13B is 32.8% helical. It is therefore likely either that substitutions interact with each other in emergent fashion or that these substitutions impact other stabilizing factors such as oligomerization.

In contrast with its effect on activity against *E. coli*, double Aib substitution was generally detrimental to FF-14 activity against *Pseudomonas* in **Figure 4B** despite strong helical character in some of these mutants. This echoed the results of **Table 1**, in which helical content was associated with activity against *E. coli* but not *Pseudomonas*, again suggesting distinct structural requirements for FF-14 killing of different gram-negative species beyond helical structure alone.

To determine whether it would be possible to substitute additional Aib mutations that might contribute to detoxification of the parent template, we made three additional mutants adding the LL-37 detoxification mutations at I9B and/or L13B to the F2B+V6B scaffold. Among these, activity remained equal to that of parent F2B+V6B when adding I9B, but with an increase of two dilutions in the threshold hemolysis level to 50 µM, thus overall yielding a 32-fold improvement in *in vitro* therapeutic index over parent LL-37 (**Figure 4C, Supplementary Table 4**). To a lesser extent, this was also true of L13B and I9B+L13B mutants within the F2B+V6B scaffold, albeit at a loss of antimicrobial potency against *E. coli* as quantified in **Supplementary Table 4**. Despite these improvements against *E. coli*, however, the Aib mutants tested again fared poorly against *Pseudomonas* (**Figure 4B**).

Thus, a combination of three Aib residues within the FF-14 scaffold can improve antimicrobial activity against *E. coli* while diminishing hemolytic activity, yielding a 32-fold improvement in *in vitro* therapeutic index. Application of these same substitutions to

Pseudomonas, however, paradoxically decreases antimicrobial potency. Understanding such distinctions in antimicrobial killing may offer a means by which to rationally target narrower spectrum antibiotics based on naturally evolved HDP templates.

Supplementary Figure 95 shows the data from **Figure 4** in histogram format. **Supplementary Figures 96-105** (antimicrobial susceptibility testing) and **106-115** (hemolysis) show the kinetic curves associated with the endpoint measures in **Figure 4**. A standardized, quantitative presentation of **Figure 4** data is provided in **Supplementary Table 4**.

Variable effect of additional modifications in Aib-induced helices

Given the ability of Aib to improve helical content, we next asked whether pairing Aib residues in the F2B+V6B scaffold with canonical amino acid substitutions might improve upon the effects of the equivalent substitutions in FF-14. Reasoning that such effects might best focus on features less likely to impact intrinsic helical character, we focused our efforts on the hydrophilic face of FF-14 as well as I9 and L13, which in LL-37 are important for oligomerization.

For certain residues, this strategy yields overall improvement. For example, while I9A ablates activity in the FF-14 template (**Figure 2**), activity of this mutant in the context of F2B+V6B is 25 μM with a neutral Fold Δ in therapeutic index relative to full-length LL-37 (**Figure 5**, **Supplementary Tables 5-6**). For most Ala mutations within the F2B+V6B scaffold, however, this overall Fold Δ goes down, driven primarily by neutral-to-decreased antimicrobial activity of mutants in the F2B+V6B scaffold compared with FF-14 – for example, at residues R8 and D11. (**Supplementary Table 6**).

Thus, despite the ability of Aib substitutions in FF-14 to support helical structure and, in the case of *E. coli*, antimicrobial activity, phenotypes may not be stable to further substitution, indicating that the underlying helix remains subject to combinatorial dynamics. Further optimization of the FF-14 template may therefore require a combinatorial approach that accounts for complex interactions among multiple substitutions while also allowing for a

combinatorial experiment matrix much larger than what can be assayed with the approaches described here. To this end, we have recently developed systems for the flow synthesis of hypervariable polyamide libraries that can support such studies[47,48].

Supplementary Figure 116 shows the data from **Figure 5** in histogram format. **Supplementary Figures 117-131** (antimicrobial susceptibility testing) and **132-146** (hemolysis) show the kinetic curves associated with the endpoint measures in **Figure 5**.

Discussion

We describe here a paired Ala-Aib structural scan of a short cathelicidin template, which was undertaken with the goal of better understanding and leveraging the relationships among cathelicidin helical structure and antimicrobial and hemolytic activities. Consistent with prior literature on full-length LL-37[20], we find that helical structure is important for cathelicidin function against *E. coli*. Surprisingly, however, we note that substitutions with Aib versus Ala at equivalent positions along the FF-14 scaffold do not correlate with activity against *Pseudomonas* (**Table 1**). This is further illustrated by selected examples within this dataset. For example, while FF-14 K10A in **Figure 2** has a 12.5 µM MIC against *Pseudomonas*, its underlying helical content is only 16.2% (**Table 1**). Substitution of that same position with Aib increases helical content to 90.3% but paradoxically raises the MIC to >50 µM (**Figure 3B**) – that is, gain of structure results in loss of function. Combined with the general observation that, as derivatives were optimized for helical content and activity against *E. coli*, they tended to lose activity against *Pseudomonas*, helical content alone may not be the sole structural driver of cathelicidin activity against gram-negative bacteria of different species. Importantly, this may suggest a means by which to intervene on cathelicidin and perhaps other HDP scaffolds to leverage differential structural activity requirements for the derivation of narrower spectrum antimicrobials.

The effects of helical content induced by Aib substitution on hemolytic activity were intermediate in this study between effects on antimicrobial activity against *E. coli* and *Pseudomonas*. We hypothesized, however, that supporting helical content while incorporating mutations at key residues corresponding to those important for oligomerization in full-length LL-37 might allow for FF-14 derivatives with improved overall *in vitro* therapeutic indices[33]. That is, in our working model, helical content may promote activity against *E. coli*, while oligomerization may promote activity against mammalian membranes.

To leverage this point, we report here a trisubstituted scaffold combining structure-promoting Aib residues at positions L2 and V6 of the FF-14 template with substitution at the I9 position, which in LL-37 is important for oligomerization and hemolytic activity. The resultant trisubstituted mutant retains antimicrobial activity against *E. coli* equivalent to FF-14 while decreasing hemolytic activity, resulting in an overall 32-fold gain in therapeutic index over LL-37. While substantial optimization lies ahead, this combines our prior work on increasing the potency of short cathelicidin derivatives into the low micromolar range typical of approved antibiotics[32] with our prior work on detoxifying full-length LL-37[33] to yield a meaningful – and perhaps more importantly, rational – improvement along the path to viable short cathelicidin therapeutics. This reliance on Aib may prove a chemically simpler method than alternatives such as chemical stapling to promote cathelicidin structure[49,50].

Despite the success of our work in the relative detoxification of an FF-14-derived scaffold using rational approaches, a consistent theme in our studies is that the FF-14 template, even when ostensibly structurally stabilized as in **Figure 5**, may not necessarily tolerate additional substitutions. To the extent that substitutions are tolerated, they may introduce emergent properties into the underlying sequence. If that is the case, the combinatorial matrix from this point forward becomes daunting for a traditional toolbox. That is, while some modifications such as N-lipidation and C-amidation that we have described previously in the context of FF-14 may be more straightforward to test[32], others that involve sequence changes

such as the use of D- amino acids or additional noncanonical residues like Aib may necessitate the exploration of massive combinatorial spaces unnavigable by standard approaches.

Anticipating such a scenario, we have recently developed methods for the rapid flow synthesis of combinatorial polyamide libraries, in part for application to problems such as this in which a large combinatorial matrix may need to be tested simultaneously via selection-based drug discovery approaches[47,48]. Using this system, we can generate chemical libraries of effectively any size up to quintillions of members with the same time and reagent usage required to make a single peptide. Current research is focused on applying concurrently developed deconvolution methods to building out a broader platform of selection systems. In principle, though, rather than individually making hundreds or thousands or millions, etc., of peptides, it may instead be possible to use saturating mutagenesis to quickly probe for all possible combinations of residues of interest that are consistent with a selectable phenotype.

In summary, we report here a paired Ala-Aib structural scan of a short cathelicidin template that reveals differential structural requirements for FF-14 activity against *E. coli*, *Pseudomonas*, and mammalian membranes. Leveraging these insights, we develop an Aib-rich short cathelicidin that partially separates antimicrobial and hemolytic activities, yielding a low micromolar MIC against *E. coli* and a 32-fold improvement in therapeutic index over the parent, naturally-occurring LL-37 sequence. This Aib-trisubstituted short cathelicidin is thus a candidate for further development of novel agents active against *Enterobacterales*, and demonstrates the feasibility of incorporating the structure-promoting features of selected natural products such as peptaibols into human HDP-derived antimicrobials.

Methods

Peptide synthesis and purification –

Peptide synthesis was completed as previously described on third generation automated flow peptide synthesizers[51–53]. Aib residues were coupled as Ala (21 strokes HATU). 4-(4-hydroxymethyl-3-methoxyphenoxy)butyric acid (HMPB) resin was used throughout (ChemMatrix). Following synthesis, peptides were cleaved with Reagent K (82.5% trifluoroacetic acid (TFA), 5% water, 5% phenol, 2.5% ethanedithiol) for 2 hours at room temperature followed by peptide precipitation in ether chilled on dry ice. Following precipitation, precipitated peptide was resuspended in 50% water / 50% acetonitrile with 0.1% TFA, flash frozen in liquid nitrogen, and lyophilized. Peptide purification was carried out on reverse phase columns with a Biotage Selekt flash chromatography system, with subsequent confirmation of the peptide identity and purity by liquid chromatography-mass spectrometry and high performance liquid chromatography. Analytical data associated with the peptides synthesized for this study are shown in the following **Supplementary Figures**: **147-157** (associated with **Figure 1**), **158-169** (associated with **Figure 2**), **170-181** (associated with **Figure 3**), **182-188** (associated with **Figure 4**), and **189-198** (associated with **Figure 5**).

Circular dichroism spectroscopy –

Peptides were dissolved in water at 0.5 mg/mL. Trifluoroethanol was then added to 20% v/v, and spectra were collected on an Aviv 420 spectrometer at 37 °C and 20 °C in 0.1 cm pathlength cuvettes. Choices of temperature in this instance represent a desire to mimic distinct physiological contexts in which LL-37 and proteolytic fragments thereof – 37 °C for most body sites and 20 °C to mimic ambient-exposed surfaces such as skin. Spectra were analyzed for secondary structural content using BeStSel[40]. The consistent application of a single system for the determination of structural content is intended here as a means of making internally

consistent relative comparisons among peptides. It is possible that helical content may differ in distinct biological contexts.

Antimicrobial susceptibility testing –

Antimicrobial susceptibility testing was completed as per Clinical & Laboratory Standards Institute guidelines with modifications previously described for cationic peptides, including the use of polypropylene plates and unadjusted Mueller Hinton Broth[54]. Protocols were scaled down to either 35 or 50 µL in 384-well plates. After plating, wells were monitored for growth by OD600 over 18 hours at 37 °C in a Tecan Spark plate reader with a Large Humidity Cassette to minimize evaporation.

Hemolysis assays –

Hemolysis assays were completed in 50 µL per well in 384-well plates in a fashion similar to antimicrobial susceptibility testing above. Defibrinated sheep blood (Hardy Diagnostics) was spun at 800 rcf for 10 minutes and washed with PBS to visual clearance. Remaining blood was then resuspended in PBS at 1% v/v. Following the addition of 25 µL of 2x target concentrations of antibiotic dissolved in PBS to 384-well plates, 25 µL of the 1% blood suspension was added for a final concentration of 0.5% v/v. Hemolysis was then monitored kinetically by OD600 in a Tecan Spark plate reader as for antimicrobial susceptibility testing. In addition to this kinetic measure, hemolysis was monitored as an endpoint measurement by the addition of 25 µL of PBS at 18 hours, spinning for 10 minutes at 800 rcf, and then removing 25 µL of supernatant to a new 384-well plate to be read at 414 nm for free hemoglobin.

Acknowledgements

This work has been funded by the National Institute of Allergy and Infectious Diseases (T32 AI007061 and K08 AI166345 to JSA; U19 AI142780 to BLP) and by the Cystic Fibrosis Foundation (ALBIN19F0, ALBIN21Q0, ALBIN22A0-KB to JSA).

Author Contributions

JSA designed and conducted experiments and wrote the paper. BLP guided the experiments and wrote the paper.

Declaration of Interests

JSA has no competing interests. BLP is a co-founder and/or member of the scientific advisory boards of several companies in the peptide and protein therapeutics space. Mass General Brigham Innovation has filed a provisional patent application that includes components of the work described here.

References

1. The Review on Antimicrobial Resistance (2014). Antimicrobial Resistance: Tackling a Crisis for the Health and Wealth of Nations. 2014.

2. Murray, C.J., Ikuta, K.S., Sharara, F., Swetschinski, L., Robles Aguilar, G., Gray, A., Han, C., Bisignano, C., Rao, P., Wool, E., et al. (2022). Global burden of bacterial antimicrobial resistance in 2019: a systematic analysis. The Lancet *399*, 629–655. https://doi.org/10.1016/S0140-6736(21)02724-0/ATTACHMENT/B227DEB3-FF04-497F-82AC-637D8AB7F679/MMC1.PDF.

3. Naghavi, M., Vollset, S.E., Ikuta, K.S., Swetschinski, L.R., Gray, A.P., Wool, E.E., Robles Aguilar, G., Mestrovic, T., Smith, G., Han, C., et al. (2024). Global burden of bacterial antimicrobial resistance 1990-2021: a systematic analysis with forecasts to 2050. Lancet *404*, 1199–1226. https://doi.org/10.1016/S0140-6736(24)01867-1.

4. Magana, M., Pushpanathan, M., Santos, A.L., Leanse, L., Fernandez, M., Ioannidis, A., Giulianotti, M.A., Apidianakis, Y., Bradfute, S., Ferguson, A.L., et al. (2020). The value of antimicrobial peptides in the age of resistance. Lancet Infect. Dis. *20*, e216–e230. https://doi.org/10.1016/S1473-3099(20)30327-3.

5. Mourtada, R., Herce, H.D., Yin, D.J., Moroco, J.A., Wales, T.E., Engen, J.R., and Walensky, L.D. (2019). Design of stapled antimicrobial peptides that are stable, nontoxic and kill antibiotic-resistant bacteria in mice. Nat. Biotechnol. *37*, 1186–1197. https://doi.org/10.1038/s41587-019-0222-z.

6. Martin-Loeches, I., Dale, G.E., and Torres, A. (2018). Murepavadin: a new antibiotic class in the pipeline. Expert Rev. Anti. Infect. Ther. *16*, 259–268. https://doi.org/10.1080/14787210.2018.1441024.

7. Srinivas, N., Jetter, P., Ueberbacher, B.J., Werneburg, M., Zerbe, K., Steinmann, J., Van der Meijden, B., Bernardini, F., Lederer, A., Dias, R.L.A., et al. (2010). Peptidomimetic antibiotics target outer-membrane biogenesis in Pseudomonas aeruginosa. Science *327*, 1010–1013. https://doi.org/10.1126/science.1182749.

8. Mookherjee, N., Anderson, M.A., Haagsman, H.P., and Davidson, D.J. (2020). Antimicrobial host defence peptides: functions and clinical potential. Nature Reviews Drug Discovery 2020 19:5 *19*, 311–332. https://doi.org/10.1038/s41573-019-0058-8.

9. Hancock, R.E.W., and Sahl, H.G. (2006). Antimicrobial and host-defense peptides as new anti-infective therapeutic strategies. Nature Biotechnology 2006 24:12 *24*, 1551–1557. https://doi.org/10.1038/nbt1267.

10. Zasloff, M. (2002). Antimicrobial peptides of multicellular organisms. Nature 2002 415:6870 *415*, 389–395. https://doi.org/10.1038/415389a.

11. Ma, X., Aminov, R., Franco, O.L., de la Fuente-Nunez, C., Wang, G., and Wang, J. (2024). Editorial: Antimicrobial peptides and their druggability, bio-safety, stability, and resistance. Front. Microbiol. *15*. https://doi.org/10.3389/FMICB.2024.1425952.

12. Wang, G., Li, X., and Wang, Z. (2016). APD3: the antimicrobial peptide database as a tool for research and education. Nucleic Acids Res. *44*, D1087–D1093. https://doi.org/10.1093/nar/gkv1278.

13. Hancock, R.E.W., Haney, E.F., and Gill, E.E. (2016). The immunology of host defence peptides: beyond antimicrobial activity. Nat. Rev. Immunol. *16*, 321–334. https://doi.org/10.1038/nri.2016.29.

14. Haney, E.F., Straus, S.K., and Hancock, R.E.W. (2019). Reassessing the Host Defense Peptide Landscape. Front. Chem. *7*, 43. https://doi.org/10.3389/fchem.2019.00043.

15. Sørensen, O.E., Follin, P., Johnsen, A.H., Calafat, J., Sandra Tjabringa, G., Hiemstra, P.S., and Borregaard, N. (2001). Human cathelicidin, hCAP-18, is processed to the antimicrobial peptide LL-37 by extracellular cleavage with proteinase 3. Blood *97*, 3951–3959. https://doi.org/10.1182/BLOOD.V97.12.3951.

16. Dürr, U.H.N., Sudheendra, U.S., and Ramamoorthy, A. (2006). LL-37, the only human member of the cathelicidin family of antimicrobial peptides. Biochimica et Biophysica Acta (BBA) - Biomembranes *1758*, 1408–1425. https://doi.org/10.1016/J.BBAMEM.2006.03.030.

17. Turner, J., Cho, Y., Dinh, N.N., Waring, A.J., and Lehrer, R.I. (1998). Activities of LL-37, a cathelin-associated antimicrobial peptide of human neutrophils. Antimicrob. Agents Chemother. *42*, 2206–2214.

18. Erriah, P., Puan, S.L., Yahaya, N.M., Wan Ahmad Kamil, W.N.I., Amin Nordin, S., Muhamad, A., and Sabri, S. (2025). Harnessing bacterial antimicrobial peptides: a comprehensive review on properties, mechanisms, applications, and challenges in combating antimicrobial resistance. J. Appl. Microbiol. *136*, 290. https://doi.org/10.1093/JAMBIO/LXAE290.

19. Andersson, D.I., Hughes, D., and Kubicek-Sutherland, J.Z. (2016). Mechanisms and consequences of bacterial resistance to antimicrobial peptides. Drug Resistance Updates *26*, 43–57. https://doi.org/10.1016/J.DRUP.2016.04.002.

20. Johansson, J., Gudmundsson, G.H., Rottenberg, M.E., Berndt, K.D., and Agerberth, B. (1998). Conformation-dependent Antibacterial Activity of the Naturally Occurring Human Peptide LL-37. Journal of Biological Chemistry *273*, 3718–3724. https://doi.org/10.1074/JBC.273.6.3718.

21. Wang, G. (2008). Structures of Human Host Defense Cathelicidin LL-37 and Its Smallest Antimicrobial Peptide KR-12 in Lipid Micelles. Journal of Biological Chemistry *283*, 32637–32643. https://doi.org/10.1074/JBC.M805533200.

22. Li, X., Li, Y., Han, H., Miller, D.W., and Wang, G. (2006). Solution structures of human ll-37 fragments and NMR-based identification of a minimal membrane-targeting antimicrobial and anticancer region. J. Am. Chem. Soc. *128*, 5776–5785. https://doi.org/10.1021/JA0584875/SUPPL_FILE/JA0584875SI20051222_013003.PDF.

23. Oren, Z., Lerman, J.C., Gudmundsson, G.H., Agerberth, B., and Shai, Y. (1999). Structure and organization of the human antimicrobial peptide LL-37 in phospholipid membranes: relevance to

the molecular basis for its non-cell-selective activity. Biochemical Journal *341*, 501. https://doi.org/10.1042/0264-6021:3410501.

24. Mishra, B., Epand, R.F., Epand, R.M., and Wang, G. (2013). Structural location determines functional roles of the basic amino acids of KR-12, the smallest antimicrobial peptide from human cathelicidin LL-37. RSC Adv. *3*, 19560–19571. https://doi.org/10.1039/C3RA42599A.

25. Lakshmaiah Narayana, J., Mechesso, A.F., Rather, I.I.G., Zarena, D., Luo, J., Xie, J., and Wang, G. (2024). Origami of KR-12 Designed Antimicrobial Peptides and Their Potential Applications. Antibiotics *13*, 816. https://doi.org/10.3390/ANTIBIOTICS13090816/S1.

26. Ajish, C., Yang, S., Kumar, S.D., Kim, E.Y., Min, H.J., Lee, C.W., Shin, S.H., and Shin, S.Y. (2022). A novel hybrid peptide composed of LfcinB6 and KR-12-a4 with enhanced antimicrobial, anti-inflammatory and anti-biofilm activities. Scientific Reports 2022 12:1 *12*, 4365-. https://doi.org/10.1038/s41598-022-08247-4.

27. Muhammad, T., Strömstedt, A.A., Gunasekera, S., and Göransson, U. (2023). Transforming Cross-Linked Cyclic Dimers of KR-12 into Stable and Potent Antimicrobial Drug Leads. Biomedicines *11*. https://doi.org/10.3390/BIOMEDICINES11020504.

28. Blasi-Romero, A., Ångström, M., Franconetti, A., Muhammad, T., Jiménez-Barbero, J., Göransson, U., Palo-Nieto, C., and Ferraz, N. (2023). KR-12 Derivatives Endow Nanocellulose with Antibacterial and Anti-Inflammatory Properties: Role of Conjugation Chemistry. ACS Appl. Mater. Interfaces *15*, 24186–24196. https://doi.org/10.1021/ACSAMI.3C04237/ASSET/IMAGES/LARGE/AM3C04237_0006.JPEG.

29. Gunasekera, S., Muhammad, T., Strömstedt, A.A., Rosengren, K.J., and Göransson, U. (2018). Alanine and Lysine Scans of the LL-37-Derived Peptide Fragment KR-12 Reveal Key Residues for Antimicrobial Activity. Chembiochem *19*, 931–939. https://doi.org/10.1002/CBIC.201700599.

30. Jacob, B., Park, I.S., Bang, J.K., and Shin, S.Y. (2013). Short KR-12 analogs designed from human cathelicidin LL-37 possessing both antimicrobial and antiendotoxic activities without mammalian cell toxicity. J. Pept. Sci. *19*, 700–707. https://doi.org/10.1002/PSC.2552.

31. Kim, E.Y., Rajasekaran, G., and Shin, S.Y. (2017). LL-37-derived short antimicrobial peptide KR-12-a5 and its D-amino acid substituted analogs with cell selectivity, anti-biofilm activity, synergistic effect with conventional antibiotics, and anti-inflammatory activity. Eur. J. Med. Chem. *136*, 428–441. https://doi.org/10.1016/j.ejmech.2017.05.028.

32. Albin, J.S., Vithanage, D.A., Johnson, C., and Pentelute, B.L. (2025). Mimicry of the LL-37 N-terminus enhances the activity of short human cathelicidin derivatives. bioRxiv, 2025.05.22.655619. https://doi.org/10.1101/2025.05.22.655619.

33. Albin, J.S., Vithanage, D.A., Vuong, W., Johnson, C., Yonker, L.M., and Pentelute, B.L. (2025). Separability of antibacterial and membranolytic activity in the human host defense peptide LL-37. bioRxiv, 2025.05.22.655608. https://doi.org/10.1101/2025.05.22.655608.

34. Karle, I.L., and Balaram, P. (1990). Structural Characteristics of α-Helical Peptide Molecules Containing Aib Residues. Biochemistry *29*, 6747–6756. https://doi.org/10.1021/BI00481A001/ASSET/BI00481A001.FP.PNG_V03.

35. De Filippis, V., De Antoni, F., Frigo, M., De Laureto, P.P., and Fontana, A. (1998). Enhanced Protein Thermostability by Ala → Aib Replacement†. Biochemistry *37*, 1686–1696. https://doi.org/10.1021/BI971937O.

36. Hirano, M., Saito, C., Goto, C., Yokoo, H., Kawano, R., Misawa, T., and Demizu, Y. (2020). Rational Design of Helix-Stabilized Antimicrobial Peptide Foldamers Containing α,α-Disubstituted Amino Acids or Side-Chain Stapling. Chempluschem *85*, 2731–2736. https://doi.org/10.1002/CPLU.202000749.

37. Toniolo, C., Crisma, M., Formaggio, F., and Peggion, C. (2001). Control of peptide conformation by the Thorpe-Ingold effect (C alpha-tetrasubstitution). Biopolymers *60*, 396–419.

38. Sancho-Vaello, E., Gil-Carton, D., François, P., Bonetti, E.J., Kreir, M., Pothula, K.R., Kleinekathöfer, U., and Zeth, K. (2020). The structure of the antimicrobial human cathelicidin LL-37 shows oligomerization and channel formation in the presence of membrane mimics. Scientific Reports 2020 10:1 *10*, 1–16. https://doi.org/10.1038/s41598-020-74401-5.

39. Sancho-Vaello, E., François, P., Bonetti, E.J., Lilie, H., Finger, S., Gil-Ortiz, F., Gil-Carton, D., and Zeth, K. (2017). Structural remodeling and oligomerization of human cathelicidin on membranes suggest fibril-like structures as active species. Sci. Rep. 7. https://doi.org/10.1038/S41598-017-14206-1.

40. Micsonai, A., Wien, F., Kernya, L., Lee, Y.H., Goto, Y., Réfrégiers, M., and Kardos, J. (2015). Accurate secondary structure prediction and fold recognition for circular dichroism spectroscopy. Proc. Natl. Acad. Sci. U. S. A. *112*, E3095–E3103. https://doi.org/10.1073/PNAS.1500851112/SUPPL_FILE/PNAS.201500851SI.PDF.

41. Vasudev, P.G., Chatterjee, S., Narayanaswamy, S., and Padmanabhan, B. (2011). Structural chemistry of peptides containing backbone expanded amino acid residues: Conformational features of β, γ, and hybrid peptides. Chem. Rev. *111*, 657–687. https://doi.org/10.1021/CR100100X/SUPPL_FILE/CR100100X_SI_002.PDF.

42. Karle, I.L., and Balaram, P. (1990). Structural Characteristics of α-Helical Peptide Molecules Containing Aib Residues. Biochemistry *29*, 6747–6756. https://doi.org/10.1021/BI00481A001/ASSET/BI00481A001.FP.PNG_V03.

43. Hou, X., Sun, R., Feng, Y., Zhang, R., Zhu, T., Che, Q., Zhang, G., and Li, D. (2022). Peptaibols: Diversity, bioactivity, and biosynthesis. Engineering Microbiology *2*, 100026. https://doi.org/10.1016/J.ENGMIC.2022.100026.

44. Sansom, M.S.P. (1993). Alamethicin and related peptaibols--model ion channels. Eur. Biophys. J. *22*, 105–124. https://doi.org/10.1007/BF00196915.

45. Degenkolb, T., Kirschbaum, J., and Brückner, H. (2007). New sequences, constituents, and producers of peptaibiotics: an updated review. Chem. Biodivers. *4*, 1052–1067. https://doi.org/10.1002/CBDV.200790096.

46. Leitgeb, B., Szekeres, A., Manczinger, L., Vágvölgyi, C., and Kredics, L. (2007). The History of Alamethicin: A Review of the Most Extensively Studied Peptaibol. Chem. Biodivers. *4*, 1027–1051. https://doi.org/10.1002/CBDV.200790095.

47. Albin, J.S., Lee, G.Y., Johnson, C., Vithanage, D.A., Vuong, W., and Pentelute, B.L. (2025). Rapid generation of hypervariable chemical libraries. Chem *0*, 102501. https://doi.org/10.1016/J.CHEMPR.2025.102501.

48. Johnson, C., Vithanage, D.A., Lee, G.Y., Pentelute, B.L., and Albin, J.S. (2025). Automated Flow Synthesis of Combinatorial Protein Libraries. https://doi.org/10.26434/CHEMRXIV-2025-MN6CT.

49. Niu, W., and Guo, J. (2024). Cellular Site-Specific Incorporation of Noncanonical Amino Acids in Synthetic Biology. Chem. Rev. https://doi.org/10.1021/ACS.CHEMREV.3C00938/ASSET/IMAGES/MEDIUM/CR3C00938_0024.GIF.

50. Biava, H.D. (2020). Tackling Achilles' Heel in Synthetic Biology: Pairing Intracellular Synthesis of Noncanonical Amino Acids with Genetic-Code Expansion to Foster Biotechnological Applications. Chembiochem *21*, 1265–1273. https://doi.org/10.1002/CBIC.201900756.

51. Albin, J.S., and Pentelute, B.L. (2020). Efficient flow synthesis of human antimicrobial peptides. Aust. J. Chem. *73*, 380–388. https://doi.org/10.1071/CH20043.

52. Hartrampf, N., Saebi, A., Poskus, M., Gates, Z.P., Callahan, A.J., Cowfer, A.E., Hanna, S., Antilla, S., Schissel, C.K., Quartararo, A.J., et al. (2020). Synthesis of proteins by automated flow chemistry. Science (1979). *368*, 980–987. https://doi.org/10.1126/science.abb2491.

53. Mijalis, A.J., Thomas, D.A., Simon, M.D., Adamo, A., Beaumont, R., Jensen, K.F., and Pentelute, B.L. (2017). A fully automated flow-based approach for accelerated peptide synthesis. Nat. Chem. Biol. *13*, 464–466. https://doi.org/10.1038/nchembio.2318.

54. Wiegand, I., Hilpert, K., and Hancock, R.E.W. (2008). Agar and broth dilution methods to determine the minimal inhibitory concentration (MIC) of antimicrobial substances. Nat. Protoc. *3*, 163–175. https://doi.org/10.1038/nprot.2007.521.

	% Helix at 37 °C				MIC *E. coli*			MIC *Pseudomonas*			20% Hemolysis			Fold Hemolysis / MIC		
	Ala	**Alb**	**% Possible**	**Fold Δ B:A**	**Ala**	**Alb**	**Fold Δ A:B**	**Ala**	**Alb**	**Fold Δ A:B**	**Ala**	**Alb**	**Fold Δ A:B**	**Ala**	**Alb**	**Fold Δ B:A**
F1	39.6	51.7	0.20	1.3	12.5	12.5	1.0	50	100	0.5	25	25	1.0	2.0	2.0	1.0
F2	16.7	74.2	0.69	4.4	25	3.1	8.0	50	25	2.0	25	12.5	2.0	1.0	4.0	4.0
I5	55.3	91.6	0.81	1.7	25	3.1	8.0	25	25	1.0	25	12.5	2.0	1.0	4.0	4.0
V6	18.7	100	1.00	5.3	12.5	3.1	4.0	25	25	1.0	25	6.3	4.0	2.0	2.0	1.0
Q7	26.5	96.5	0.95	3.6	6.3	3.1	2.0	12.5	12.5	1.0	6.3	6.3	1.0	1.0	2.0	2.0
R8	100	100	n/a	1.0	3.1	3.1	1.0	25	50	0.5	6.3	3.1	2.0	2.0	1.0	0.5
I9	8.1	54	0.50	6.7	100	12.5	8.0	50	25	2.0	200	50	4.0	2.0	4.0	2.0
K10	16.2	90.3	0.88	5.6	12.5	3.1	4.0	50	100	0.5	6.3	1.6	4.0	0.5	0.5	1.0
D11	92.7	68.7	n/a	0.7	3.1	3.1	1.0	6.3	6.3	1.0	3.1	6.3	0.5	1.0	2.0	2.0
F12	75.9	84.7	0.37	1.1	12.5	12.5	1.0	25	25	1.0	50	25	2.0	4.0	2.0	0.5
L13	10.3	18.2	0.09	1.8	50	50	1.0	25	25	1.0	200	100	2.0	4.0	2.0	0.5
R14	16	74.1	0.69	4.6	6.3	6.3	1.0	50	50	1.0	12.5	12.5	1.0	2.0	2.0	1.0
Avg	39.7	75.3	0.62		22.4	9.6		32.8	39.1		48.7	21.7		1.9	2.3	
			Avg Δ	3.2		Avg Δ	3.3		Avg Δ	1.0		Avg Δ	2.1		Avg Δ	1.6

Table 1 – Paired Ala-Aib helix scanning distinguishes the effects of helical content on FF-14 functional activities. Table 1 summarizes the quantitative effects of replacing a given residue in FF-14 with Aib in place of Ala. Antimicrobial activity against *E. coli* tracks closely with increased helical content, while antimicrobial activity against *Pseudomonas* does not. Hemolytic activity demonstrates intermediate dependence, allowing for a modest increase in overall therapeutic index as measured against the *E. coli* MIC throughout this paper. % Helix at 37 °C shows the percentage of helical content in each peptide as calculated by BeStSel based on the spectra shown in **Supplementary Figures 58** and **92**. % Possible divides the absolute % helix change observed by the total possible % helix change (to a maximum of 100%) to account for different baseline helical content among peptides. Fold-change is derived by dividing the Aib percentage by the Ala percentage. MIC indicates the minimum inhibitory concentrations of each peptide against *E. coli* or *Pseudomonas* as shown in **Figures 2** and **3** and associated **Supplementary Figures**, with the fold change derived by dividing the Ala MIC by the Aib MIC, such that larger numbers indicate more potent antimicrobial activity in Aib mutants. 20% Hemolysis indicates the highest peptide concentration with less than 20% hemolysis as shown in **Figures 2** and **3** and associated **Supplementary Figures**, with the fold change derived by dividing the Ala concentration by the Aib concentration, such that larger numbers indicate more toxic activity in Aib-containing derivatives. Fold Hemolysis / MIC indicates the ratio of the 20% Hemolysis threshold for each peptide divided by the MIC for each peptide against *E. coli*. The fold change is derived by dividing the Aib ratio by the Ala ratio, such that larger numbers indicate improved *in vitro* therapeutic indices.

A.

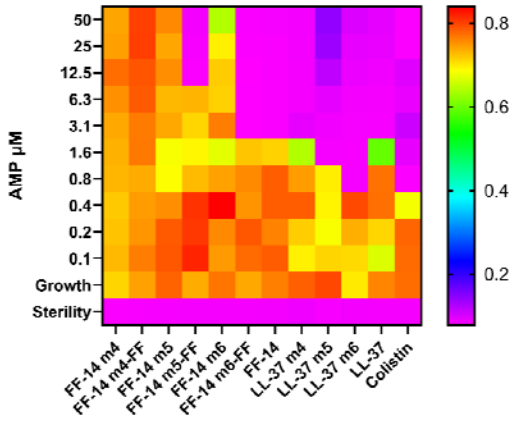
AMP µM
50
25
12.5
6.3
3.1
1.6
0.8
0.4
0.2
0.1
Growth
Sterility
FF-14 m4
FF-14 m4-FF
FF-14 m5
FF-14 m5-FF
FF-14 m6
FF-14 m6-FF
FF-14
LL-37 m4
LL-37 m5
LL-37 m6
LL-37
Colistin
0.8
0.6
0.4
0.2

B.

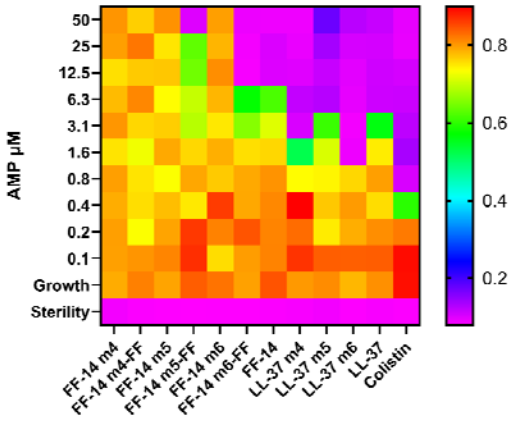
AMP µM
50
25
12.5
6.3
3.1
1.6
0.8
0.4
0.2
0.1
Growth
Sterility
FF-14 m4
FF-14 m4-FF
FF-14 m5
FF-14 m5-FF
FF-14 m6
FF-14 m6-FF
FF-14
LL-37 m4
LL-37 m5
LL-37 m6
LL-37
Colistin
0.8
0.6
0.4
0.2

C.

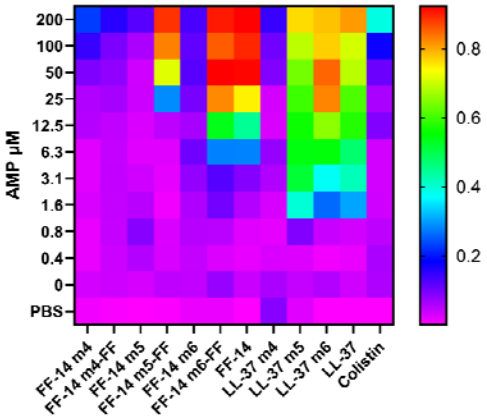
AMP µM
200
100
50
25
12.5
6.3
3.1
1.6
0.8
0.4
0
PBS
FF-14 m4
FF-14 m4-FF
FF-14 m5
FF-14 m5-FF
FF-14 m6
FF-14 m6-FF
FF-14
LL-37 m4
LL-37 m5
LL-37 m6
LL-37
Colistin
0.8
0.6
0.4
0.2

D.

FF-14 m4 AAKRAAQRAKDFAR
FF-14 m4-FF FFKRAAQRAKDFAR
FF-14 m5 EFKRIVARIADFLA
FF-14 m5-FF FFKRIVARIADFLA
FF-14 m6 EFKRIVQAIKAALR
FF-14 m6-FF FFKRIVQAIKAALR
FF-14 FFKRIVQRIKDFLR
LL-37 m4 LLGDFFRKAKEKAGKAAKRAAQRAKDFARNLVPRTES
LL-37 m5 LLGDFFRKSKEKIGKEFKRIVARIADFLANLVPRTES
LL-37 m6 LLGDFFRKSKEKIGKEFKRIVQAIKAALRAAVPRTES
LL-37 LLGDFFRKSKEKIGKEFKRIVQRIKDFLRNLVPRTES

E.

H
F
F
K
R
I
V
Q
R
I
K
D
F
L
R
OH

Figure 1 – Antimicrobial and hemolytic activities correlate in grouped Ala mutants of FF-14. A-B. Antimicrobial susceptibility testing of *E. coli* (**A**) and *Pseudomonas* (**B**) was carried out using a series of grouped Ala mutants based on those previously used in full-length LL-37. In contrast with the separation of antibacterial and hemolytic functions in LL-37 m4 as well as in the control antibiotic colistin, antibacterial and hemolytic functions typically correlate among FF-14 grouped Ala mutant derivatives. Data show the raw OD600 after 18 hours of incubation at 37 °C; warm colors indicate bacterial growth, while cool colors are low / no growth. **C.** Hemolytic activity of each of the tested FF-14 derivatives as assessed by hemoglobin release after 18 hours of incubation at 37 °C. Cool colors indicate low signal at 414 nm, while warm colors are high signal; numbers are scaled to a 100% freeze-thaw hemolysis control. **D.** Sequence alignment showing each of the FF-14 mutants in **A-C** as well as the parent LL-37 mutants used as controls. **E.** Schematic depiction of the FF-14 scaffold.

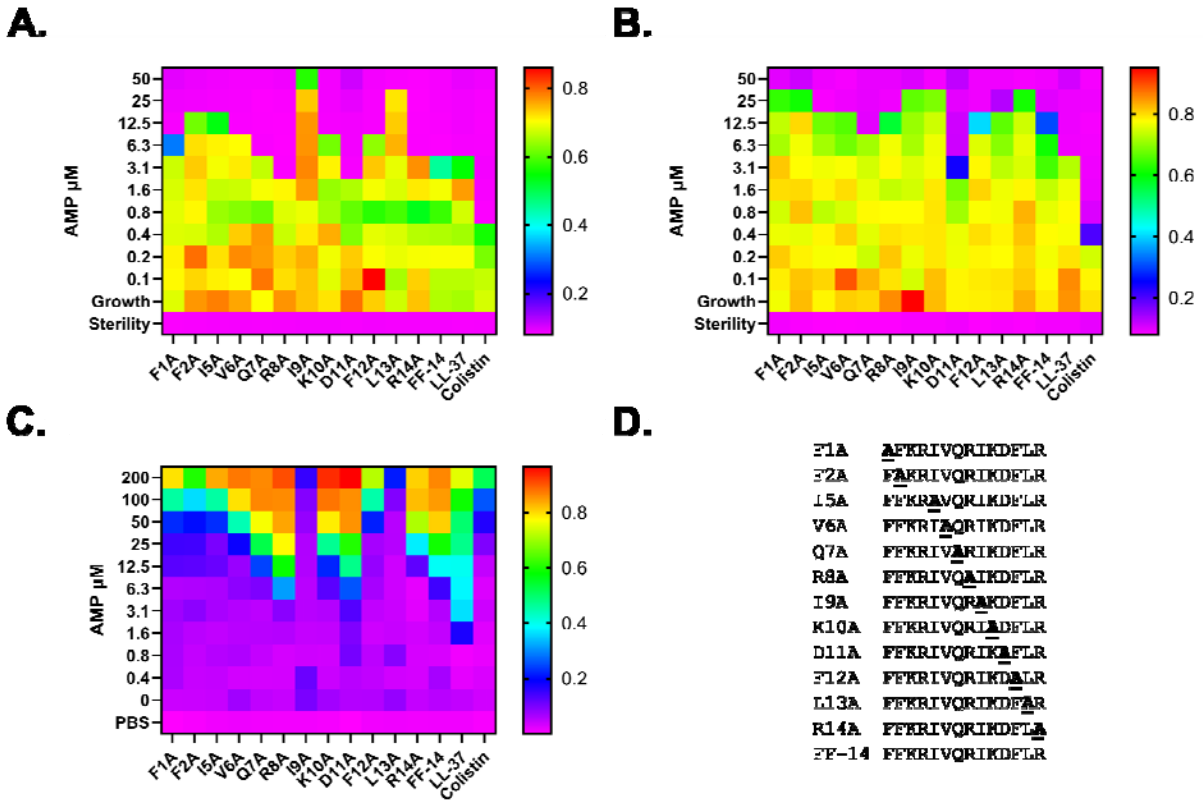
A.
B.
C.
D.
AMP µM
50
25
12.5
6.3
3.1
1.6
0.8
0.4
0.2
0.1
Growth
Sterility
200
100
0
PBS
F1A
F2A
I5A
V6A
Q7A
R8A
I9A
K10A
D11A
F12A
L13A
R14A
FF-14
LL-37
Colistin
0.8
0.6
0.4
0.2
F1A AFKRIVQRIKDFLR
F2A FAKRIVQRIKDFLR
I5A FFKRAVQRIKDFLR
V6A FFKRIAQRIKDFLR
Q7A FFKRIVARIKDFLR
R8A FFKRIVQAIKDFLR
I9A FFKRIVQRAKDFLR
K10A FFKRIVQRIADFLR
D11A FFKRIVQRIKAFLR
F12A FFKRIVQRIKDALR
L13A FFKRIVQRIKDFAR
R14A FFKRIVQRIKDFLA
FF-14 FFKRIVQRIKDFLR

Figure 2 – Antimicrobial and hemolytic activities of FF-14 single Ala mutants correlate with each other. A-B. Antimicrobial susceptibility testing of *E. coli* (**A**) and *Pseudomonas* (**B**) was carried out using a series of single Ala mutants in FF-14. Data show the raw OD600 after 18 hours of incubation at 37 °C; warm colors indicate high signal representing bacterial growth, while warm colors are low signal and growth. **C.** Hemolytic activity of each of the tested FF-14 derivatives as assessed by hemoglobin release after 18 hours of incubation at 37 °C. Cool colors indicate low signal at 414 nm, while warm colors are high signal; numbers are scaled to a 100% freeze-thaw hemolysis control. **D.** Sequence alignment showing each of the FF-14 mutants in **A-C**.

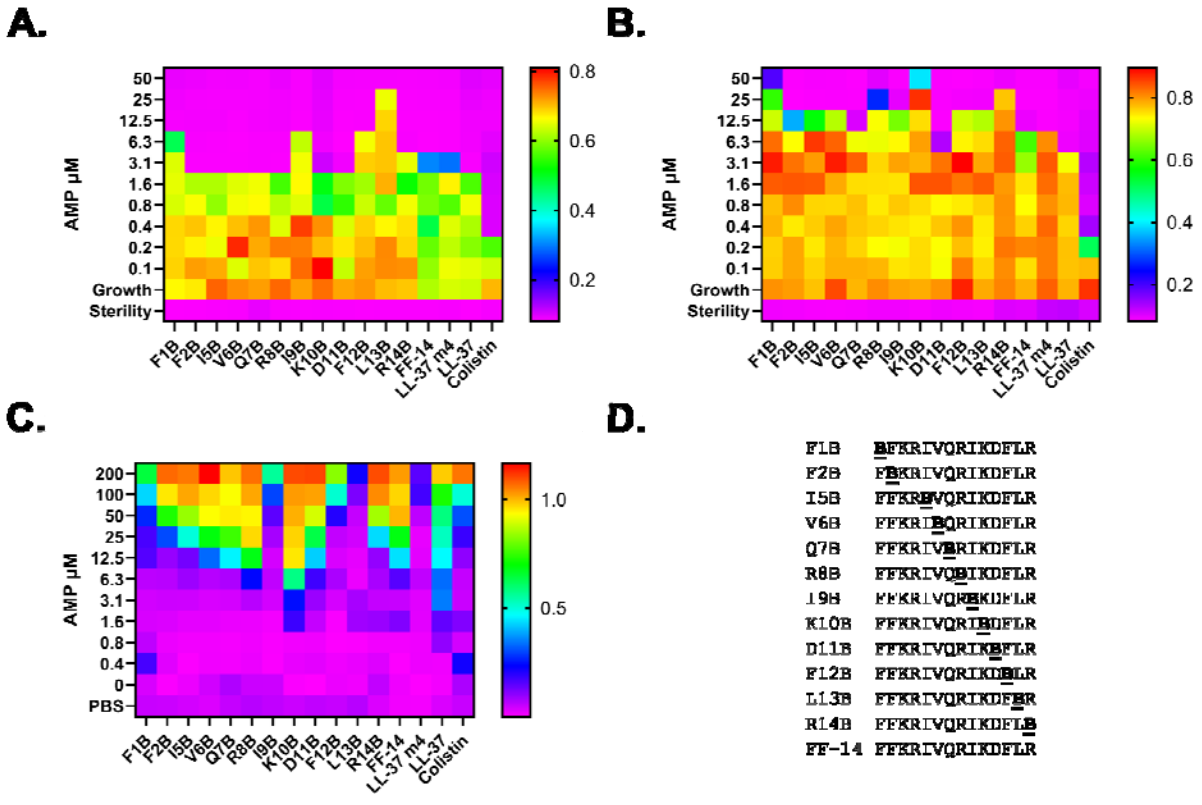
A.
B.
C.
D.
AMP µM
50
25
12.5
6.3
3.1
1.6
0.8
0.4
0.2
0.1
Growth
Sterility
200
100
0
PBS
F1B
F2B
I5B
V6B
Q7B
R8B
I9B
K10B
D11B
F12B
L13B
R14B
FF-14
LL-37 m4
LL-37
Colistin
0.8
0.6
0.4
0.2
1.0
0.5
F1B BFKRIVQRIKDFLR
F2B FBKRIVQRIKDFLR
I5B FFKRBVQRIKDFLR
V6B FFKRIBQRIKDFLR
Q7B FFKRIVBRIKDFLR
R8B FFKRIVQBIKDFLR
I9B FFKRIVQRBKDFLR
K10B FFKRIVQRIBDFLR
D11B FFKRIVQRIKBFLR
F12B FFKRIVQRIKDBLR
L13B FFKRIVQRIKDFBR
R14B FFKRIVQRIKDFLB
FF-14 FFKRIVQRIKDFLR

Figure 3 – Aib substitution improves FF-14 antimicrobial activity against *E. coli*, but not *Pseudomonas*. Although MICs were notably decreased against *E. coli* on substitution with Aib along the length of FF-14, this effect was no observed on MICs against *Pseudomonas*. **A-B.** Antimicrobial susceptibility testing of *E. coli* (**A**) and *Pseudomonas* (**B**) was carried out using a series of single Aib mutants in FF-14. Data show the raw OD600 after 18 hours of incubation at 37 °C; warm colors indicate high signal representing bacterial growth, while warm colors are low signal and growth. **C.** Hemolytic activity of each of the tested FF-14 derivatives as assessed by hemoglobin release after 18 hours of incubation at 37 °C. Cool colors indicate low signal at 414 nm, while warm colors are high signal; numbers are scaled to a 100% freeze-thaw hemolysis control. **D.** Sequence alignment showing each of the FF-14 mutants in **A-C**.

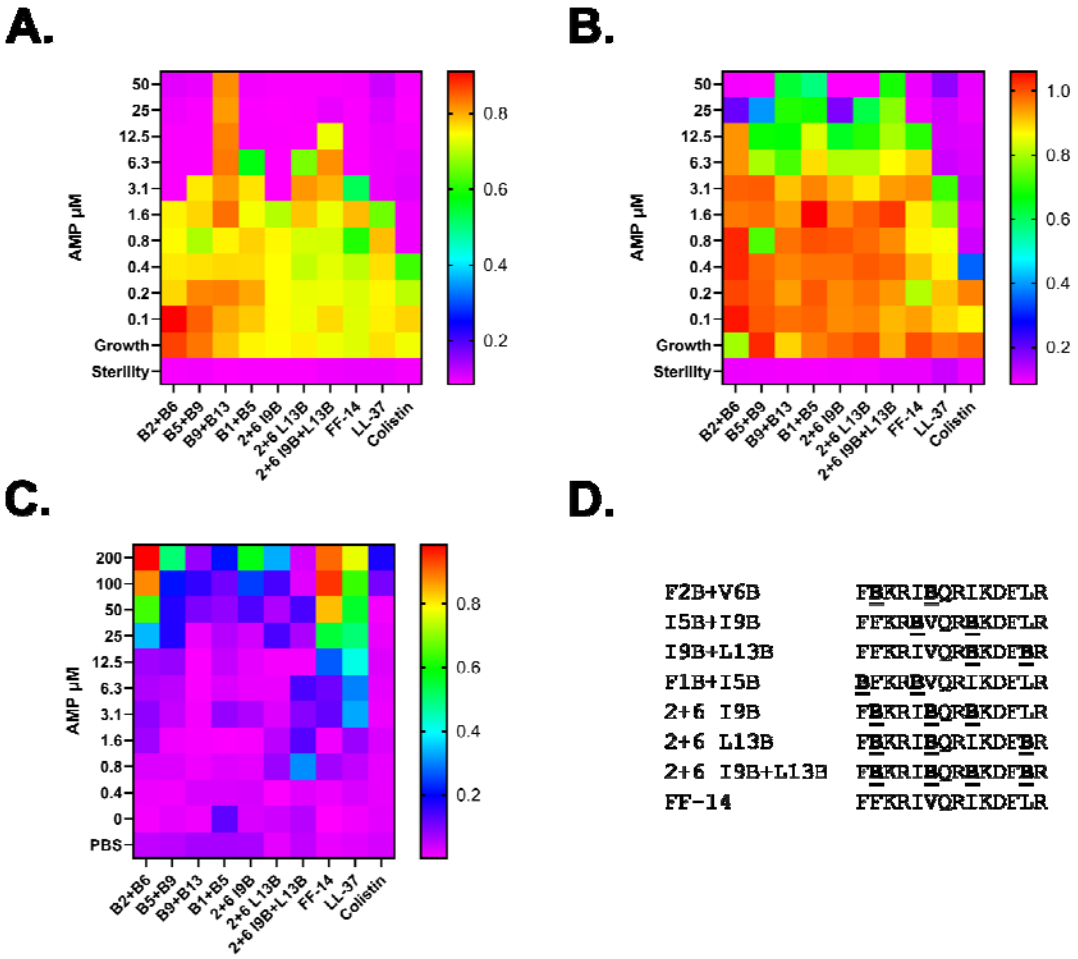
A.
AMP µM
50
25
12.5
6.3
3.1
1.6
0.8
0.4
0.2
0.1
Growth
Sterility
B2+B6
B5+B9
B9+B13
B1+B5
2+6 I9B
2+6 L13B
2+6 I9B+L13B
FF-14
LL-37
Colistin
0.8
0.6
0.4
0.2
B.
AMP µM
1.0
0.8
0.6
0.4
0.2
C.
AMP µM
200
100
50
25
12.5
6.3
3.1
1.6
0.8
0.4
0
PBS
0.8
0.6
0.4
0.2
D.
F2B+V6B FBKRIBQRIKDFLR
I5B+I9B FFKRBVQRBKDFLR
I9B+L13B FFKRIVQRBKDFBR
F1B+I5B BFKRBVQRIKDFLR
2+6 I9B FBKRIBQRBKDFLR
2+6 L13B FBKRIBQRIKDFBR
2+6 I9B+L13B FBKRIBQRBKDFBR
FF-14 FFKRIVQRIKDFLR

Figure 4 – A modified FF-14 scaffold F2B+V6B with an additional I9B modification retains antimicrobial activity against *E. coli* while demonstrating diminished hemolytic activity. The F2B+V6B retains a low-micromolar MIC against *E. coli* while demonstrating diminished hemolytic activity, leading to an overall 32-fold increase in *in vitro* therapeutic index over the parent LL-37 peptide (see also **Supplementary Table 4**). Activity of multiply-Aib substituted peptides against *Pseudomonas*, however, was generally poor. **A-B.** Antimicrobial susceptibility testing of *E. coli* (**A**) and *Pseudomonas* (**B**) was carried out using a series of single 2-4 Aib mutations in FF-14. Data show the raw OD600 after 18 hours of incubation at 37 °C; warm colors indicate higher bacterial growth, while warm colors are low / no growth. **C.** Hemolytic activity of each of the tested FF-14 derivatives as assessed by hemoglobin release after 18 hours of incubation at 37 °C. Cool colors indicate low signal at 414 nm, while warm colors are high signal; numbers are scaled to a 100% freeze-thaw hemolysis control. **D.** Sequence alignment showing each of the FF-14 Aib mutants in **A-C**.

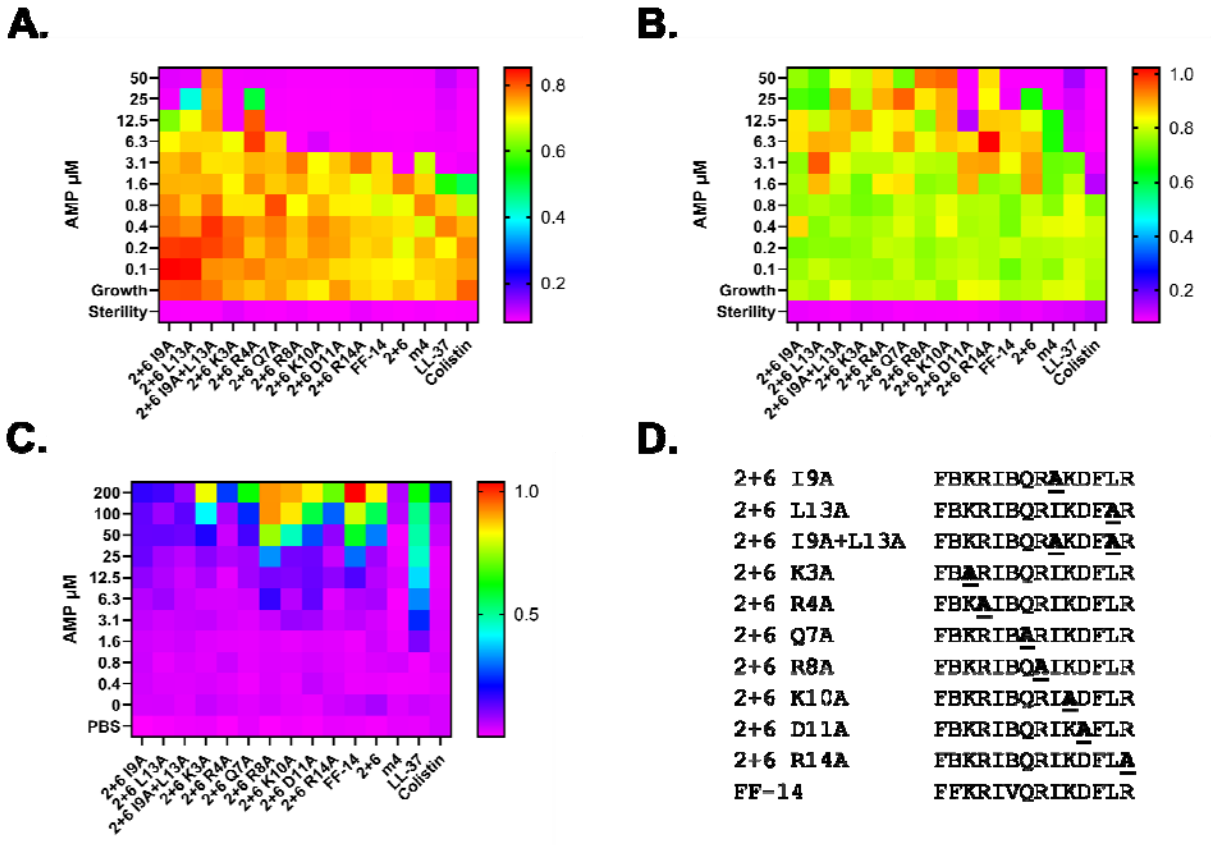
A.
B.
C.
D.
AMP µM
50
25
12.5
6.3
3.1
1.6
0.8
0.4
0.2
0.1
Growth
Sterility
200
100
0
PBS
2+6 I9A
2+6 L13A
2+6 I9A+L13A
2+6 K3A
2+6 R4A
2+6 Q7A
2+6 R8A
2+6 K10A
2+6 D11A
2+6 R14A
FF-14
2+6
m4
LL-37
Colistin
0.8
0.6
0.4
0.2
1.0
0.5
2+6 I9A FBKRIBQRAKDFLR
2+6 L13A FBKRIBQRIKDFAR
2+6 I9A+L13A FBKRIBQRAKDFAR
2+6 K3A FBARIBQRIKDFLR
2+6 R4A FBKAIBQRIKDFLR
2+6 Q7A FBKRIBARIKDFLR
2+6 R8A FBKRIBQAIKDFLR
2+6 K10A FBKRIBQRIADFLR
2+6 D11A FBKRIBQRIKAFLR
2+6 R14A FBKRIBQRIKDFLA
FF-14 FFKRIVQRIKDFLR

Figure 5 – Variable effect of additional modifications in Aib-induced helices. While activity of some derivatives such as F2B+V6B + I9A is improved against *E. coli* over the equivalent FF-14 I9A mutant, other substitutions such as R8A and D11A no longer improve upon the antimicrobial activity of the parent scaffold. Activity against *Pseudomonas* is generally poor. **A-B.** Antimicrobial susceptibility testing of *E. coli* (**A**) and *Pseudomonas* (**B**) was carried out using a series of single Ala mutations in FF-14 F2B+V6B. Data show the raw OD600 after 18 hours of incubation at 37 °C; warm colors indicate high signal representing bacterial growth, while warm colors are low signal and growth. **C.** Hemolytic activity of each of the tested FF-14 derivatives as assessed by hemoglobin release after 18 hours of incubation at 37 °C. Cool colors indicate low signal at 414 nm, while warm colors are high signal; numbers are scaled to a 100% freeze-thaw hemolysis control. **D.** Sequence alignment showing each of the mutants in **A-C**.